

# Hyperspectral Imaging: A New Approach to the Diagnosis of Hemorrhagic Shock

Leopoldo C. Cancio, MD, Andriy I. Batchinsky, MD, James R. Mansfield, MSc, Svetlana Panasyuk, PhD, Katherine Hetz, BS, David Martini, MS, Bryan S. Jordan, RN, MSN, Brian Tracey, PhD, and Jenny E. Freeman, MD

**Background:** Skin color changes and mottling are frequently described signs of hemorrhagic shock (HEM). Based on this, we developed a noninvasive, noncontact hyperspectral imaging system (HSI), which quantifies and depicts the surface tissue saturation of oxygen ( $S_{\text{HSI}O_2}$ ) for each pixel in a region of interest (ROI). Our purpose was to assess HSI in a porcine HEM model. We hypothesized that HEM would cause decreases in  $S_{\text{HSI}O_2}$  of the skin.

**Methods:** The HyperMed HSI system employs a spectral separator to vary the wavelength of light admitted to a digital camera. During image acquisition, a “hypercube” of images, each at a separate wavelength, is generated (at 5-nm intervals, from 500 to 600 nm). Then, the visible light spectrum for each pixel in the hypercube is compared by linear regression to standard

spectra for oxyhemoglobin (OxyHb) and deoxyhemoglobin (DeoxyHb). The resulting fit coefficients for OxyHb and DeoxyHb are used to calculate  $S_{\text{HSI}O_2}$  values for each pixel in the ROI. The mean values for OxyHb, DeoxyHb, and  $S_{\text{HSI}O_2}$  across the ROI are calculated. Grayscale  $S_{\text{HSI}O_2}$  pictures of the ROI are also generated, in which the brightness of each pixel is proportional to its value. Seventeen pigs,  $36.4 \pm 0.11$  kg, underwent standard preparation, and were maintained on ketamine and isoflurane. Normothermia was maintained ( $37^\circ\text{C}$  to  $39^\circ\text{C}$ ). The hemorrhage group (HEM,  $n = 9$ ) underwent three blood withdrawals, each 10 mL/kg, with 15 minutes between withdrawals. After the third withdrawal, animals were resuscitated with lactated Ringer’s and then shed blood. The control group (CTRL,

$n = 8$ ) received intravenous fluids at 100 mL/h. HSI images were obtained of the inner hindlimb throughout.

**Results:** All HEM animals showed linear decreases in both mean  $S_{\text{HSI}O_2}$  and OxyHb values with blood loss, which were reversed by resuscitation. These changes were evident on the grayscale  $S_{\text{HSI}O_2}$  pictures, but not to the naked eye, and paralleled those of invasively obtained arterial base excess and mixed venous oxygen saturation.

**Conclusions:** HSI is a promising noninvasive and noncontact tool for quantifying changes in skin oxygenation during HEM and resuscitation.

**Key Words:** Hemorrhagic shock, Diagnostic imaging, Spectrum analysis, Skin, Hemoglobins, Oxyhemoglobins, Pig.

*J Trauma.* 2006;60:1087–1095.

Changes in skin color and mottling of the skin are frequently mentioned as important clinical findings in critically ill patients: “Decreased perfusion of the skin can be an early sign of shock . . . Mottling, pallor, delayed capillary refill, and peripheral cyanosis often indicate poor skin perfusion.”<sup>1</sup> However, no objective method of quantifying such findings currently exists; furthermore, these changes

may be absent or undetectable to the naked eye in a large number of patients. The goal of this study was to assess the utility of a novel technology, hyperspectral imaging (HSI), for noncontact, noninvasive monitoring of the skin during hemorrhagic shock and resuscitation. By quantifying and depicting spatial changes in hemoglobin oxygen saturation in the skin, HSI takes advantage of the fact that the skin is readily available, potentially providing a “window” through which to view systemic physiology. This application of HSI also exploits the responsiveness of the cutaneous circulation to hypovolemia.

HSI is a method of “imaging spectroscopy.” Spectroscopy is widely used to monitor metabolic status in a variety of tissues. For example, spectroscopic methods are incorporated in pulse oximeters, which utilize the different oxy- and deoxyhemoglobin absorption bands to estimate arterial oxygen saturation.<sup>2</sup> Point spectroscopy in the near infrared range interrogates the tissue saturation of oxygen in subcutaneous tissue, muscle, and/or brain, and has been used for patient monitoring in hemorrhagic shock, in extremity compartment syndrome, and following head trauma.<sup>3–7</sup>

Point spectroscopy systems do not provide information about the spatial distribution of the data. Such spatial information is provided by HSI, and could constitute a potential

Submitted for publication May 6, 2005.

Accepted for publication February 8, 2006.

Copyright © 2006 by Lippincott Williams & Wilkins, Inc.

From the US Army Institute of Surgical Research (L.C.C., A.I.B., K.H., D.M., B.S.J.), Fort Sam Houston, Texas; and HyperMed, Inc. (J.R.M., S.P., B.T., J.E.F.), Watertown, Massachusetts.

The opinions or assertions contained herein are the private views of the authors and are not to be construed as official or as reflecting the views of the Department of the Army or the Department of Defense.

This study was funded by Technologies for Metabolic Monitoring 2002, DAMD 17-02-1-0714, and by the Combat Casualty Care Research Program, US Army Medical Research and Materiel Command.

Presented as a poster at the 18th Annual Meeting of the Eastern Association for the Surgery of Trauma, January 12–15, 2005, Ft. Lauderdale, Florida.

Address for Reprints: COL Leopoldo C. Cancio, US Army Institute of Surgical Research, 3400 Rawley E., Chambers Avenue, Fort Sam Houston, TX 78234-6315; email: lee.cancio@amedd.army.mil.

DOI: 10.1097/01.ta.0000217357.10617.3d

Report Documentation Page				Form Approved OMB No. 0704-0188	
Public reporting burden for the collection of information is estimated to average 1 hour per response, including the time for reviewing instructions, searching existing data sources, gathering and maintaining the data needed, and completing and reviewing the collection of information. Send comments regarding this burden estimate or any other aspect of this collection of information, including suggestions for reducing this burden, to Washington Headquarters Services, Directorate for Information Operations and Reports, 1215 Jefferson Davis Highway, Suite 1204, Arlington VA 22202-4302. Respondents should be aware that notwithstanding any other provision of law, no person shall be subject to a penalty for failing to comply with a collection of information if it does not display a currently valid OMB control number.					
1. REPORT DATE <b>01 MAY 2006</b>		2. REPORT TYPE <b>N/A</b>		3. DATES COVERED <b>-</b>	
4. TITLE AND SUBTITLE <b>Hyperspectral imaging: a new approach to the diagnosis of hemorrhagic shock</b>				5a. CONTRACT NUMBER	
				5b. GRANT NUMBER	
				5c. PROGRAM ELEMENT NUMBER	
6. AUTHOR(S) <b>Cancio, L. C. Batchinsky, A. I. Mansfield, J. R. Panasyuk, S. Hetz, K. Martini, D. Jordan, B. S. Tracey, B. Freeman, J. E.</b>				5d. PROJECT NUMBER	
				5e. TASK NUMBER	
				5f. WORK UNIT NUMBER	
7. PERFORMING ORGANIZATION NAME(S) AND ADDRESS(ES) <b>United States Army Institute of Surgical Research, JBSA Fort Sam Houston, TX 78234</b>				8. PERFORMING ORGANIZATION REPORT NUMBER	
9. SPONSORING/MONITORING AGENCY NAME(S) AND ADDRESS(ES)				10. SPONSOR/MONITOR'S ACRONYM(S)	
				11. SPONSOR/MONITOR'S REPORT NUMBER(S)	
12. DISTRIBUTION/AVAILABILITY STATEMENT <b>Approved for public release, distribution unlimited</b>					
13. SUPPLEMENTARY NOTES					
14. ABSTRACT					
15. SUBJECT TERMS					
16. SECURITY CLASSIFICATION OF:			17. LIMITATION OF ABSTRACT <b>SAR</b>	18. NUMBER OF PAGES <b>9</b>	19a. NAME OF RESPONSIBLE PERSON
a. REPORT <b>unclassified</b>	b. ABSTRACT <b>unclassified</b>	c. THIS PAGE <b>unclassified</b>			

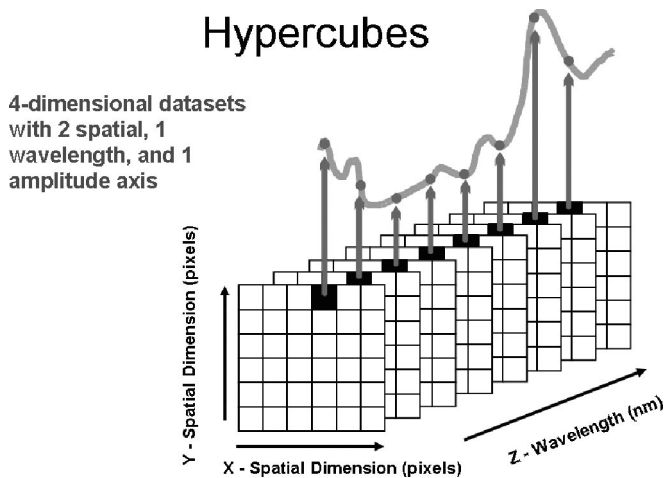


**Fig. 1.** Hyperspectral imaging generates a four-dimensional data-set, termed an image cube or hypercube. This consists of two spatial dimensions (the x and y coordinates of each pixel in the region of interest); one wavelength dimension; and one amplitude dimension. In other words, for each pixel in the region, the visible light spectrum is recorded.

advantage of the latter approach. In HSI, the spectrum of reflected light is acquired for each pixel in a region, and each such spectrum is subjected to standard spectral analysis (Fig. 1). This allows the creation of an image based on the chemical content of the region of interest (ROI).

Used for decades in airborne systems for the analysis of geological features, HSI has recently been applied to biomedicine.<sup>8</sup> It has been employed in microscopic studies of histologic sections.<sup>9,10</sup> In vivo, HSI has been used to demonstrate the macroscopic distribution of skin oxygen saturation in models of ischemia-reperfusion, following nitric oxide inhalation and inhibition, and in patients with sickle cell disease and with diabetic foot ulcers.<sup>11–14</sup> One application of HSI has been in the early prediction of tissue viability following plastic surgery: tissue that has insufficient oxygenation to remain viable is readily apparent from oxygen saturation maps calculated from near-infrared spectral images acquired immediately following surgery. By contrast, clinical signs of impending necrosis do not become apparent to the naked eye for 6 to 12 hour after surgery.<sup>15,16</sup> Assessment of tissue viability following burns has also been performed.<sup>17,18</sup>

We recently developed a system capable of hyperspectral imaging in the visible light wavelength range. In a porcine pilot study, we previously used this system to observe changes in cutaneous oxygen saturation following chest trauma and hemorrhage, which were not evident to the naked eye, but which produced hyperspectral images with a pronounced mottling pattern.<sup>19</sup> Based on this experience, we hypothesized that the image intensity of hyperspectral oxygen saturation images of the skin would decrease during hemorrhagic shock in a porcine model, indicating a decrease in oxygen saturation in the skin. We also sought to gain initial experience with HSI during hypothermia, to determine

whether this common complication of hemorrhagic shock and resuscitation would alter the HSI images. Our ultimate goal is to develop a system that demonstrates blood-loss induced changes earlier than other modalities, or which provides data which are otherwise unavailable, to facilitate rapid diagnosis and directed treatment of shock.

## MATERIALS AND METHODS

This study was approved by the Institutional Animal Care and Use Committee. All animals were cared for in accordance with the guidelines set forth by the Animal Welfare Act and other federal statutes and regulations relating to studies involving animals, and by the 1996 *Guide for the Care and Use of Laboratory Animals* of the National Research Council. All animals were maintained in a facility approved by the International Association for the Assessment and Accreditation of Laboratory Animal Care.

### Hemorrhagic Shock Study

Seventeen female Yorkshire pigs (nine in the hemorrhage group and eight in the control group), weighing  $36.4 \pm 0.11$  kg were used in this study. The animals were quarantined for 1 week and were fasted overnight before the experiment.

Animals were premedicated with 250 mg IM Telazol (Lederle Parenterals, Inc. Carolina, PR). After induction of anesthesia with isoflurane delivered through a mask, they were intubated, and were placed on a Datex-Ohmeda anesthesia ventilator with a tidal volume of 10 mL/kg and a respiratory rate of 12/min. The rate was adjusted to achieve normocapnea ( $\text{PaCO}_2 = 35$  to 45 mm Hg). Anesthesia was maintained with a mixture of isoflurane (2% to 2.5%) and room air. Percutaneous sheath introducers (8.5 Fr; Arrow International, Reading, PA) were inserted into the carotid artery and external jugular vein bilaterally, and a 10-F Foley catheter was inserted into the urinary bladder. A splenectomy was performed via a midline laparotomy. The splenic artery was tied off before splenectomy to allow drainage of blood from the spleen into the circulation. An infusion of lactated Ringer's solution (LR) at 1.5 times the spleen weight was administered immediately after the splenectomy. At the end of surgery the isoflurane was decreased to 0.6% and an infusion of ketamine (250 to 350  $\mu\text{g/kg/min}$ ) was begun. The ketamine-isoflurane anesthesia and room-air mechanical ventilation were continued until the end of the study. Depth-of-anesthesia assessment and anesthetic dose adjustments were made as needed. Core temperature was maintained between 37°C to 39°C by means of an external heating pad (Gayman Industries, New York, NY).

A flow-directed pulmonary artery catheter (VIP Oximetry 782HF75, Edwards Life Sciences, Irvine, CA) was inserted via the external jugular vein introducer sheath to permit measurement of mixed venous blood gases and core temperature. One of the carotid arterial introducer sheaths was used for measurement of the arterial blood pressure (ABP). Clinical pressure transducers (Transpac IV trifurcated monitoring kit, Abbott

**Table 1** Experimental Schedule, Hemorrhage Study

Time Point	Event
1	Blood transfusion
2	Bleed 1
3	Postbleed 1
4	Bleed 2
5	Postbleed 2
6	Bleed 3
7	Postbleed 3
8	LR resuscitation
9	Post-LR
10	Blood transfusion
11	Posttransfusion
12	End of study

Bleed, periods during which 10 mL/kg blood was removed (10 min each); postbleed, periods of observation following bleed periods; LR, lactated ringer's solution; blood transfusion, reinfusion of shed blood.

Critical Care Systems, Abbott Laboratories, North Chicago, IL) were used. The heart rate was obtained from the electrocardiogram. Regional skin temperature was monitored on both hindlimbs using thermocouples (Physiotemp BAT- 10, Type T thermocouple thermometer system, Physiotemp Instruments, Clifton, NJ).

The experimental schedule is given in Table 1. After a postoperative stabilization period (1 to 2 hours), baseline data were collected. The animals in the hemorrhage group then underwent withdrawal of blood through the carotid line with a syringe. Three withdrawals, each 10 mL/kg, were performed at a constant rate of 1 mL/kg/min. Blood was collected into a bag containing CPDA anticoagulant (J-520 blood collection unit, Jorgensen Laboratories, Loveland, CO). Each of the three 10-minute hemorrhage periods was followed by a 15-minute observation period. Following the third observation period, the animals were resuscitated with intravenous infusion of LR at 1.5 times the shed blood volume. The duration of the LR resuscitation period was 25 minutes. Additional fluid to exceed the initial resuscitation volume was then administered as needed to return the heart rate and blood pressure toward baseline values. The 25-minute LR infusion period was followed by a 30-minute observation period, and then a 25-minute period during which the shed blood was reinfused. The animals were observed for an additional hour thereafter and then were euthanized. Blood and LR were infused using a fluid warmer (Ranger blood/fluid warming system, Model 254, Augustine Medical, Prairie, MN).

Animals in the control group underwent similar surgical preparation and received a maintenance LR infusion at 100 mL/h. Data were obtained at the following time points: baseline, after each 10 mL/kg blood withdrawal, after LR resuscitation, and after blood reinfusion.

## Hyperspectral Imaging

Hyperspectral images were collected using a 10-bit Kodak MegaPlus 1.6i digital camera, consisting of a 1024 × 1532 pixel charge-coupled device (CCD) element and a 10-

bit A/D converter (Roper Scientific, Trenton, NJ). The camera was fitted with an AF 50-mm f/2.8 EX Macro camera lens (Sigma Corporation, Tokyo, Japan). Wavelength selection was provided by a visible-wavelength, liquid-crystal tunable filter (VIS2, Cambridge Research and Instrumentation, Woburn, MA) with a nominal 7-nm bandpass. This filter was fitted to the front of the camera lens (Fig. 2). By varying the voltage across the liquid crystal tunable filter, the wavelength of light admitted through the filter, and into the camera, can be varied. A 100-W quartz-halogen light powered from a Sorenson 150-W DC power supply (Elgar Electronics, San Diego, CA) was used to provide coaxial illumination for the camera system. Custom software was developed under the LabVIEW system (National Instruments Corporation, Austin, TX) to control the image acquisition hardware and process.

Images of the proximal inner hindlimb were collected at 5-nm intervals from 500 to 600 nm, with the integration times adjusted such that the brightest image in each sequence filled approximately 80% of the full well capacity of the CCD. The data resulting from one of these sequences is known as an image cube or "hypercube," each of which requires approximately 2 minutes to acquire (Fig. 1). Fiduciary marks were placed on the skin with an indelible black marker to facilitate image registration.

Images were collected as full 1024 × 1532 pixel arrays, and then were binned down to 256 × 382 arrays. Background images were subtracted from each image in the image cube. The data were then converted to optical density units by dividing the sample data by data acquired from a white reflectance standard using a Beer's Law algorithm. A complete description of this methodology can be found elsewhere<sup>20</sup> and in Appendix 1.

## Imaging System

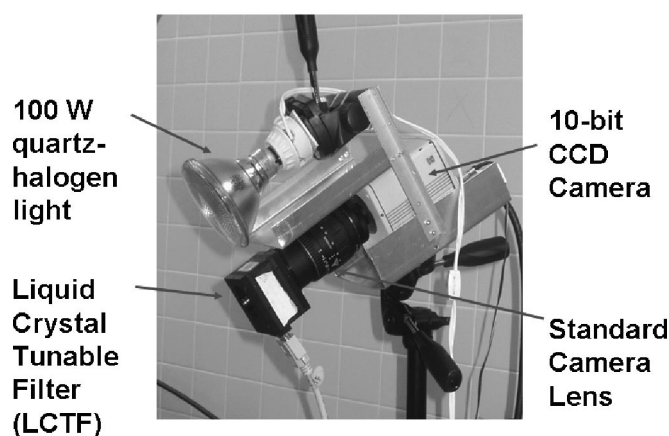


**Fig. 2.** The hyperspectral imaging system consists of an illumination source and a digital charge-coupled device (CCD) camera. In front of the camera, a liquid crystal tunable filter is used to vary the wavelength of light admitted to the camera. During the acquisition of one hypercube, the voltage is varied, stepwise, across the filter—a process which takes about 2 minutes. At each new voltage, an image at a different wavelength of light is obtained.

Briefly, reference oxyhemoglobin and deoxyhemoglobin spectra were obtained in electronic format.<sup>21</sup> A four-term linear regression fitting of oxyhemoglobin, deoxyhemoglobin, offset and slope terms was then performed on each of the spectra in the image cube. The regression fit coefficients were then used to calculate the relative oxygen saturation percentage for each spectrum in the image cube:

$$S_{\text{HbO}_2} = \text{OxyHb} / (\text{OxyHb} + \text{DeoxyHb}) \times 100,$$

where OxyHb is the fit coefficient for oxyhemoglobin, and DeoxyHb is the fit coefficient for deoxyhemoglobin, resulting from the linear regression.<sup>19</sup> The mean values for  $S_{\text{HbO}_2}$ , for OxyHb, and for DeoxyHb were calculated across the entire ROI of each image at each timepoint, yielding variables which were then subjected to further statistical analysis by conventional methods (see below). In addition, grayscale images were generated in which the brightness of each pixel is proportionate to the  $S_{\text{HbO}_2}$  value for that pixel. All spectral computations were done using Matlab (The Mathworks, Natick, MA).

### Laser Doppler Imaging

A raster-optics-based Laser Doppler Perfusion Imager (Periscan PIM II, Perimed AB, Stockholm, Sweden) was used to obtain images based on noncontact laser Doppler flowmetry of the region of interest (ROI). Mean perfusion was calculated off line for  $16 \times 16$  pixel windows within the ROI.

### Assays

Arterial and mixed venous blood samples were collected into preheparinized 1-mL disposable syringes at each sampling time point. They were analyzed using an AVL Omni Modular System (Roche Diagnostics GmbH Graz, Austria).

### Statistical Analysis

Statistical analysis employed SPSS v. 10.1 (SPSS Inc., Chicago, IL) and Microsoft Excel 2000 (Microsoft Corp., Redmond, WA). Independent-sample *t* tests were used to compare control versus hemorrhage animals at each timepoint. Linear regression was used to compare continuous variables. For the hyperspectral variables, bivariate Pearson correlation coefficients were calculated for each animal over time in the hemorrhage group, from baseline to time point 7 (postbleed 3). Significance was accepted at  $p < 0.05$ . Data are presented as means  $\pm$  SEM.

## RESULTS

As can be seen in Table 2, blood withdrawal resulted in an early drop in systolic arterial pressure, which became statistically significant in comparison with the control group during the first withdrawal, and which remained decreased until after LR resuscitation. The heart rate increased with blood withdrawal, although in delayed fashion—becoming

significant only during the second bleed; it returned to control levels after reinfusion of shed blood. Other physiologic parameters are given in Table 2.

Oxygen saturation images in which the brightness of each pixel is proportionate to the intensity of the  $S_{\text{HbO}_2}$  for that pixel are shown in Figure 3. Here, both baseline images and images obtained during the third postbleed period are included. The decrease in image intensity is evident on these images. Qualitatively, some animals, but not all, demonstrated an increase in mottling during shock, also evident on the oxygen saturation images. Neither of these changes was evident to the naked eye. Quantitatively, the mean  $S_{\text{HbO}_2}$  value for these images decreased linearly with blood withdrawal, becoming significantly decreased in comparison with control animals after the third bleed, and restored to control levels by resuscitation (Fig. 4, Table 2). The mean value of the OxyHb fit coefficient for the ROI also decreased linearly with hemorrhage, but it showed an earlier statistically significant decrease, after the second bleed, which was also restored by resuscitation (Fig. 5, Table 2). Meanwhile, the mean DeoxyHb fit coefficient for the ROI trended upward during and after the third bleed, but these changes were not significant (Fig. 6, Table 2).

Pearson correlation coefficients were calculated for each animal's individual hyperspectral variables over time points 1 to 7 (baseline to postbleed 3). These results are given in Table 3. Note that the correlation coefficients for the primary end-point variable,  $S_{\text{HbO}_2}$ , ranged from  $-0.755$  to  $-0.976$  (mean  $-0.863$ ); in other words, this variable showed the expected linear decrease in  $S_{\text{HbO}_2}$  with hemorrhage in all cases. Likewise, all but one animal demonstrated the expected linear decrease in OxyHb with hemorrhage. By contrast, results for DeoxyHb, although positive as expected for all animals, were more variable.

The SD of the  $S_{\text{HbO}_2}$  images, a rough index of the degree of mottling present, did not change significantly (data not shown). Laser Doppler imaging demonstrated a linear decrease in skin blood flow for the ROI with blood loss, which became significant after the third bleed and which was reversed by resuscitation (Table 2).

Linear regression was performed to examine the possible relationship between mixed venous saturation of oxygen and  $S_{\text{HbO}_2}$ . This analysis demonstrated a linear relationship, with a relatively low  $r^2$  of 0.12 ( $p < 0.001$ ,  $df = 114$ ). Correlation with the systolic arterial pressure was similar ( $r^2 = 0.14$ ,  $p < 0.001$ ,  $df = 202$ ). Although the laser Doppler image intensity appeared to follow a time course similar to that of  $S_{\text{HbO}_2}$ , there was no relationship between the two variables on linear regression ( $r^2 = 0.01$ ,  $p = 0.312$ ,  $df = 112$ ).

## DISCUSSION

The principal finding in this study is that the mean intensities of both  $S_{\text{HbO}_2}$  and OxyHb images of the skin, obtained by hyperspectral imaging in the visible wavelength range, decreased during hemorrhagic shock and were restored

**Table 2** Physiologic and Hyperspectral Data

Variable	Group	1	2	3	4	5	6	7	8	9	10	11	12
SAP	Control	94 ± 3	97 ± 2	97 ± 2	99 ± 3	99 ± 4	101 ± 4	98 ± 4	99 ± 3	93 ± 2	94 ± 3	91 ± 3	87 ± 3
	Bleed	96 ± 3	78 ± 5*	78 ± 4*	67 ± 5*	71 ± 5*	56 ± 4*	65 ± 9*	90 ± 6	82 ± 7	87 ± 5	104 ± 6	102 ± 6
DAP	Control	67 ± 3	69 ± 2	70 ± 2	72 ± 2	72 ± 3	72 ± 3	72 ± 3	70 ± 2	68 ± 2	65 ± 2	63 ± 2	59 ± 4
	Bleed	70 ± 3	52 ± 4*	53 ± 4*	45 ± 3*	49 ± 4*	35 ± 3*	41 ± 7*	55 ± 6*	51 ± 7*	61 ± 6	75 ± 7	73 ± 7
CVP	Control	4 ± 1	4 ± 0	4 ± 1	4 ± 1	4 ± 1	4 ± 1	4 ± 1	4 ± 1	4 ± 1	4 ± 1	4 ± 1	5 ± 1
	Bleed	4 ± 1	4 ± 1	4 ± 1	2 ± 1	2 ± 1	2 ± 1	3 ± 1	6 ± 2	4 ± 1	7 ± 2	9 ± 1*	6 ± 1
Heart rate	Control	99 ± 4	97 ± 4	96 ± 4	96 ± 4	96 ± 4	94 ± 3	93 ± 3	92 ± 2	92 ± 2	94 ± 3	94 ± 3	93 ± 3
	Bleed	97 ± 4	97 ± 5	103 ± 4	124 ± 10*	136 ± 11*	155 ± 11*	168 ± 10*	135 ± 7*	124 ± 6*	118 ± 7*	103 ± 4	106 ± 8
SPAP	Control	22 ± 1	22 ± 1	21 ± 1	22 ± 1	21 ± 1	22 ± 1	21 ± 1	22 ± 1	21 ± 1	22 ± 1	22 ± 1	22 ± 1
	Bleed	20 ± 1	18 ± 1*	18 ± 1	16 ± 1*	14 ± 2*	14 ± 1*	18 ± 2	25 ± 3	21 ± 2	28 ± 3	30 ± 2*	28 ± 2*
DPAP	Control	9 ± 1	10 ± 1	10 ± 1	10 ± 1	10 ± 1	11 ± 1	10 ± 1	11 ± 1	11 ± 1	11 ± 1	12 ± 1	12 ± 1
	Bleed	9 ± 1	9 ± 1	9 ± 1	8 ± 1	7 ± 1	6 ± 1	7 ± 2	13 ± 1	10 ± 1	16 ± 2	16 ± 2	17 ± 2
SvO <sub>2</sub>	Control	72.1 ± 1.8		75.6 ± 1.9		71.6 ± 3.1		72.3 ± 1.9		72.0 ± 1.5		68.9 ± 2.4	69.1 ± 3.0
	Bleed	70.9 ± 2.5		64.8 ± 4.4		50.5 ± 4.5*		36.6 ± 5.9*		53.6 ± 4.5*		69.1 ± 2.6	64.2 ± 3.7
Arterial BE	Control	4.2 ± 0.7		4.1 ± 0.5		4.6 ± 0.5		4.9 ± 0.5		4.9 ± 0.4		4.4 ± 0.5	4.3 ± 0.6
	Bleed	4.3 ± 0.8		2.5 ± 1.3		2.2 ± 0.9*		-1.0 ± 2.2*		-1.0 ± 2.1*		1.3 ± 1.9	2.9 ± 1.8
Arterial Hb	Control	10.4 ± 0.2		10.5 ± 0.3		10.5 ± 0.2		10.5 ± 0.3		10.6 ± 0.3		10.6 ± 0.3	10.5 ± 0.3
	Bleed	11.0 ± 0.3		10.1 ± 0.5		10.0 ± 0.2		9.3 ± 0.3*		7.0 ± 0.3*		9.5 ± 0.3*	9.7 ± 0.3*
Temp PA	Control	37.1 ± 0.3	37.2 ± 0.3	37.2 ± 0.4	37.3 ± 0.4	37.3 ± 0.4	37.3 ± 0.4	37.3 ± 0.4	37.3 ± 0.4	37.4 ± 0.4	37.4 ± 0.4	37.5 ± 0.4	37.6 ± 0.4
	Bleed	36.8 ± 0.2	36.9 ± 0.1	36.9 ± 0.1	37.0 ± 0.1	37.0 ± 0.1	37.1 ± 0.2	37.1 ± 0.2	37.0 ± 0.2	37.1 ± 0.2	37.2 ± 0.2	37.2 ± 0.2	37.3 ± 0.2
DeoxyHb	Control	0.45 ± 0.03	0.45 ± 0.02	0.45 ± 0.02	0.46 ± 0.02	0.46 ± 0.03	0.46 ± 0.03	0.47 ± 0.02	0.46 ± 0.03	0.46 ± 0.03	0.46 ± 0.03	0.46 ± 0.02	0.46 ± 0.03
	Bleed	0.42 ± 0.01	0.43 ± 0.01	0.42 ± 0.01	0.43 ± 0.02	0.43 ± 0.02	0.47 ± 0.03	0.50 ± 0.04	0.40 ± 0.02	0.39 ± 0.01*	0.40 ± 0.02	0.42 ± 0.01	0.42 ± 0.02
OxyHb	Control	0.14 ± 0.01	0.15 ± 0.01	0.16 ± 0.01	0.16 ± 0.01	0.16 ± 0.01	0.16 ± 0.01	0.16 ± 0.01	0.17 ± 0.01	0.17 ± 0.01	0.17 ± 0.01	0.18 ± 0.01	0.19 ± 0.02
	Bleed	0.16 ± 0.01	0.14 ± 0.01	0.14 ± 0.01	0.13 ± 0.01	0.13 ± 0.01*	0.12 ± 0.01*	0.11 ± 0.01*	0.14 ± 0.01	0.14 ± 0.01	0.14 ± 0.01	0.17 ± 0.01	0.18 ± 0.02
S <sub>HIS</sub> O <sub>2</sub>	Control	24 ± 2	26 ± 2	26 ± 2	26 ± 2	26 ± 2	26 ± 2	26 ± 2	27 ± 2	28 ± 2	28 ± 2	28 ± 2	29 ± 3
	Bleed	27 ± 1	25 ± 1	25 ± 1	23 ± 1	22 ± 1	20 ± 2	19 ± 1*	26 ± 2	27 ± 1	27 ± 1	28 ± 1	30 ± 3
Laser Doppler	Control	1.10 ± 0.09		1.10 ± 0.08		1.10 ± 0.08		1.06 ± 0.07		1.14 ± 0.05		1.10 ± 0.07	1.10 ± 0.06
	Bleed	0.96 ± 0.09		0.83 ± 0.07*		0.78 ± 0.07*		0.66 ± 0.05*		0.90 ± 0.12		0.91 ± 0.13	0.91 ± 0.13

See Table 1 for explanation of experimental time points.

\* Significant difference between control and bleed groups by independent samples t test at this time point,  $p < 0.05$ .

SAP, systolic arterial pressure; DAP, diastolic arterial pressure; CVP, central venous pressure; SPAP, systolic pulmonary arterial pressure; DPAP, diastolic pulmonary arterial pressure; SvO<sub>2</sub>, mixed venous saturation of oxygen; arterial BE, arterial base excess; arterial Hb, arterial hemoglobin; temp PA, temperature of pulmonary arterial blood; OxyHb, mean value of the oxyhemoglobin fit coefficient for the region of interest; DeoxyHb, mean value of the deoxyhemoglobin fit coefficient for the region of interest; S<sub>HIS</sub>O<sub>2</sub>, mean value of the oxygen saturation of hemoglobin for the region of interest; laser Doppler, laser Doppler image intensity.

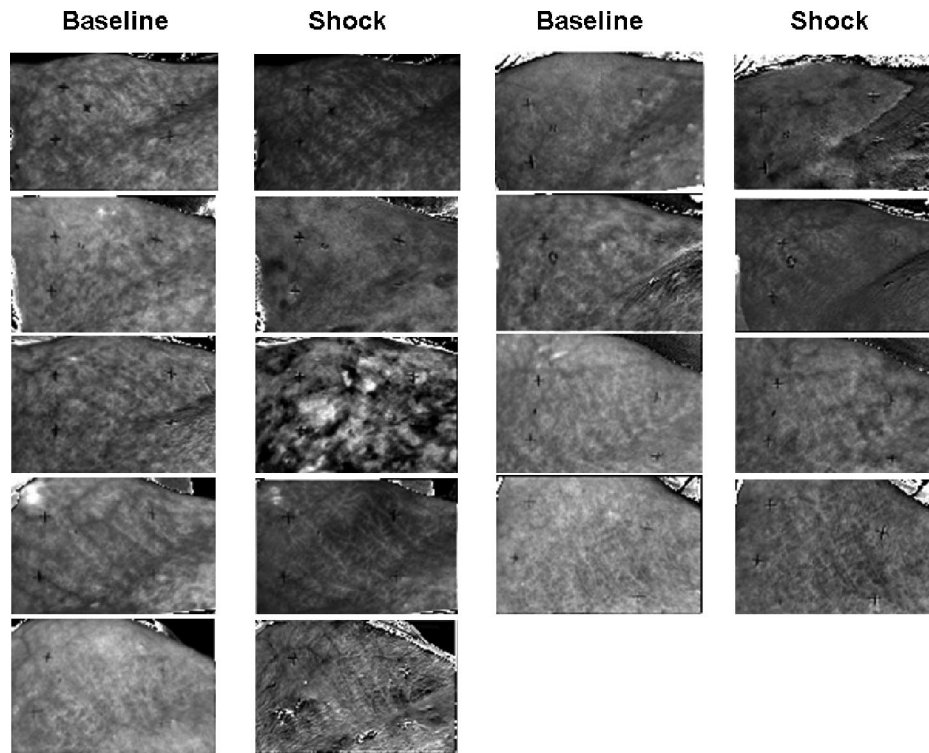


**Fig. 3.** These images were generated by calculating the  $S_{\text{HSI}}\text{O}_2$  value for each pixel in the field of view. Then, each pixel was given a grayscale brightness value proportionate to the  $S_{\text{HSI}}\text{O}_2$  value. The resulting images are shown. Clear differences in  $S_{\text{HSI}}\text{O}_2$  are evident between baseline images and those produced after the third bleed. In addition, some animals demonstrated an increase in regional heterogeneity, or mottling—most notably the third animal on the left. These changes were not evident to the naked eye.

during resuscitation in anesthetized pigs. These changes roughly paralleled those observed in several invasively obtained variables, to include the systolic arterial pressure, the arterial base excess, and the mixed venous saturation of oxygen. Thus, HSI may be a useful, noninvasive method of monitoring the response to shock and the adequacy of resuscitation.

Systolic blood pressure dropped more rapidly than did the other variables, including the mean  $S_{\text{HSI}}\text{O}_2$  and OxyHb variables. The rapidity of this drop in blood pressure during relatively moderate blood loss, coupled by a delay in the compensatory tachycardic response to the decrease, indicates that cardiovascular compensation for hemorrhage may have been impaired in this anesthetized porcine model. The depressive effects of general anesthesia on sympathetic nervous

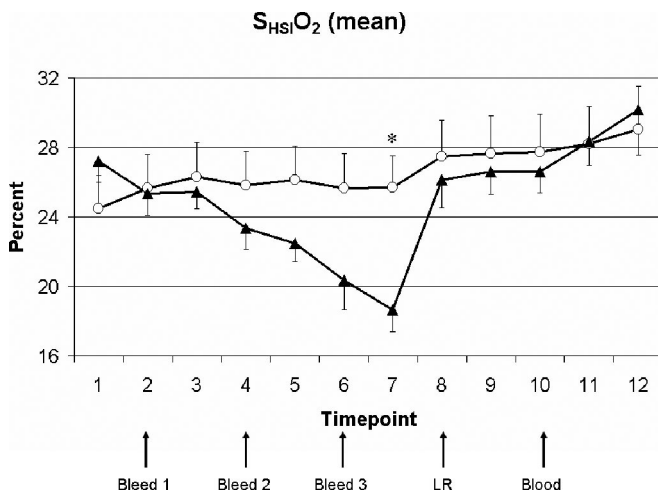


**Fig. 4.** The mean  $S_{\text{HSI}}\text{O}_2$  for the region of interest was calculated and is shown here.  $S_{\text{HSI}}\text{O}_2$  decreased linearly with blood withdrawal and became significantly different from control values after the third bleed.

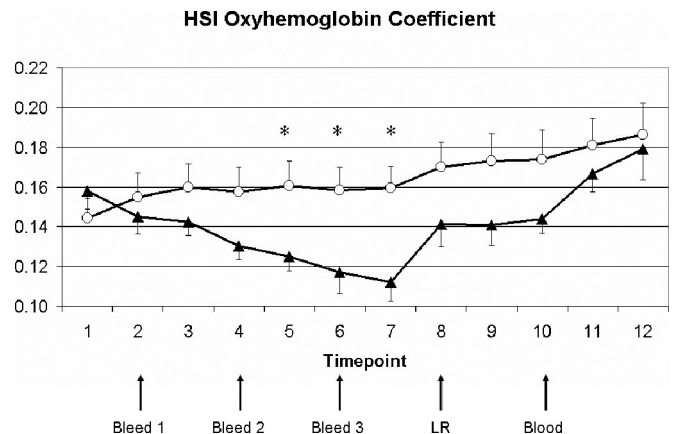


**Fig. 5.** The mean OxyHb fit coefficient for the same region of interest is shown here. This value also decreased linearly with hemorrhage and became significantly different from control values after the second bleed.

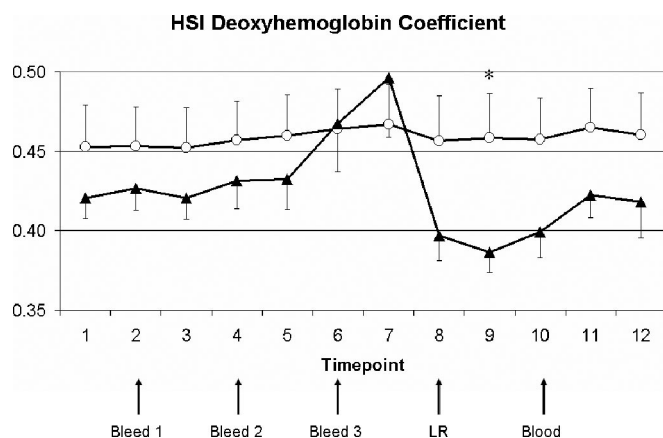


**Fig. 6.** The mean DeoxyHb fit coefficient increased with hemorrhage, but this change was not statistically significant in comparison with control animals.

system activity, on peripheral vascular responsiveness, on cutaneous vasoconstriction, on baroreflex sensitivity, and on cardiac function are well known.<sup>22–26</sup> These effects limit the applicability of models which employ general anesthesia, such as that used in the present study, to conscious human trauma patients. Recently, we have improved the image registration capabilities of the HSI system, such that immobilization of subjects by means of general anesthesia should not be required for future studies. Whether studies in unanesthetized subjects would reveal increased sensitivity to lower volumes of blood loss, and whether HSI would be superior to traditional vital signs under those circumstances, remains to be determined.

Mottling was inconsistently observed in these hyperspectral images, in contrast to the pronounced increase in mottling which we previously observed in a single case of chest trauma and hemorrhage.<sup>19</sup> The reasons for this are unclear.

**Table 3** Pearson Correlation Coefficients and Hyperspectral Data

Subject	OxyHb PC	Mean Sig	DeoxyHb PC	Mean Sig	S <sub>HSI</sub> O <sub>2</sub> PC	Mean Sig
1	−0.898	0.006	0.659	0.108	−0.872	0.011
2	0.562	0.189	0.874	0.010	−0.755	0.050
3	−0.994	<0.001	0.107	0.819	−0.970	<0.001
4	−0.727	0.064	0.792	0.034	−0.828	0.021
5	−0.954	0.001	0.648	0.115	−0.921	0.003
6	−0.653	0.112	0.557	0.194	−0.704	0.077
7	−0.922	0.003	0.925	0.003	−0.939	0.002
8	−0.976	<0.001	0.401	0.373	−0.976	<0.001
9	−0.905	0.005	0.077	0.870	−0.804	0.029

For each animal in the hemorrhage group were analyzed over time points 1 to 7.

OxyHb mean, mean value of the oxyhemoglobin fit coefficient for the region of interest; DeoxyHb mean, mean value of the deoxyhemoglobin fit coefficient for the region of interest; S<sub>HSI</sub>O<sub>2</sub> mean, mean value of the oxygen saturation of hemoglobin for the region of interest; PC, Pearson correlation coefficient; sig, two-tailed significance level.

However, anesthesia may also impair the control mechanisms for cutaneous blood flow, causing a dampening of the blood flow oscillations which normally occur in response to hypovolemia. Braverman and colleagues described the relationship between the microanatomy of the cutaneous circulation and regional heterogeneity in blood flow by laser Doppler flowmetry.<sup>27–30</sup> They also described synchronicity in cutaneous blood-flow oscillations between sites on ipsilateral and contralateral limbs, suggesting that such oscillations are controlled centrally by the sympathetic nervous system. Indeed, stimulation of the lumbar sympathetic trunk at appropriate frequencies increases the amplitude of skin blood-flow oscillations measured by laser Doppler.<sup>31</sup> Such increases in vasomotion may play a protective role, by enabling red blood cells to traverse the microvasculature under conditions of increased vascular resistance.<sup>32</sup> Further studies employing HSI in unanesthetized humans undergoing lower body negative pressure are being conducted, and may determine whether an increase in regional heterogeneity in S<sub>HSI</sub>O<sub>2</sub> images is a prominent feature of the response to central hypovolemia. In addition, novel image analysis methods of detecting and quantifying such mottling are being developed. Finally, direct measurement of cutaneous sympathetic nerve activity would shed light on control of the cutaneous circulation during shock.<sup>33</sup>

Thermoregulation is a major function of the cutaneous circulation,<sup>34,35</sup> and hypothermia is commonly present in trauma casualties. Thus, the relationship between systemic hypothermia and localized cutaneous oxygen saturation is relevant to an assessment of HSI technology. We were concerned that hypothermia would activate cutaneous sympathetic nerves and cause a reduction in cutaneous blood flow; in fact, this response can be used as a test of the integrity of the autonomic nervous system.<sup>36,37</sup> In turn, a reduction in cutaneous blood flow could cause a decrease in skin oxygen saturation, assuming local metabolic demands remained constant. The decrease in mean S<sub>HSI</sub>O<sub>2</sub> and OxyHb values during the hemorrhagic shock study were not caused by systemic hypothermia; core and skin temperature were maintained during the experiment.

In a separate pilot study, moderate and profound hypothermia did not appear to produce similar effects (data not shown). Possibly, decreased metabolic demands defended against desaturation during moderate and profound hypothermia. However, further research would be needed to evaluate fully the effect of hypothermia on HSI.

The technology used in this study performed imaging in the visible wavelength range of 500 to 600 nm. This wavelength selection provides improved signal-to-noise ratio over near-infrared spectroscopy for the measurement of hemoglobin spectra, because the hemoglobin absorption signal is much stronger in the visible than in the near-infrared range. The utility of near-infrared point spectroscopy lies in its ability to provide information about subsurface tissue oxygenation, for example in brain or muscle, and which derives

from the increased tissue penetration of near-infrared light<sup>3–7</sup>. By contrast, visible light spectroscopy, as employed in this study, interrogates hemoglobin saturation at a more superficial level, most likely within dermal capillaries. Near-infrared spectroscopy can also be used to measure tissue water content.<sup>38</sup> Thus, visible and near infrared approaches provide potentially complementary information. Furthermore, technology that simultaneously performs hyperspectral imaging in both the near infrared and visible ranges is under development. In darkly pigmented subjects, epidermal melanin dominates the visible light spectrum. Several studies suggest that this may not impair the ability of HSI systems to characterize changes in cutaneous oxygen saturation.<sup>12,14,39</sup>

Calibration of this HSI system was performed using reference spectra.<sup>21</sup> Direct measurement of OxyHb and DeoxyHb levels in skin has not been performed in conjunction with HSI. It can be seen (Figs. 5 and 6) that there was more variability in DeoxyHb than in OxyHb levels in control animals, and in both values in control animals as compared with hemorrhaged animals. Whether the changes in OxyHb and DeoxyHb levels seen in this study are clinically significant—whether, for example, certain values are associated with survival—can only be determined by more work in animals and humans.

Laser Doppler imaging is another approach to imaging the skin during shock and resuscitation. Light and colleagues have envisioned the use of this technology as a guide to resuscitation following thermal injury.<sup>40</sup> HSI and laser Doppler imaging are different technologies, the former providing information about tissue oxygenation and the latter about blood flow. Further improvements in HSI may offer advantages over currently available laser Doppler imagers with respect to image resolution and acquisition time. In conclusion, we have developed a hyperspectral imaging system which demonstrates changes in skin oxygen saturation during hemorrhagic shock and resuscitation. Further studies are planned to elucidate fully the potential of this new technology.

## APPENDIX 1: IMAGE PROCESSING

The following is a more detailed description of the HSI process used in this study, adopted from Gillies et al.<sup>19</sup> Raw sample images (S) and reference images (R) were smoothed using a three-point mean filter along spectral dimension of the image cubes. The smoothed sample image cubes (S) were ratioed against the smoothed reference image cubes (R) to convert the data to an optical density scale (A). The optical density at pixel i,j (A<sub>ij</sub>) of each raw image was calculated by:

$$A_{ij} = -\log_{10}(S_{ij}/R_{ij}) \quad (1)$$

The conversion of the data to optical density allowed the spectra to be analyzed using standard spectroscopic algorithms.<sup>20</sup> Linear regression fit coefficients c<sub>1</sub>, c<sub>2</sub>, and c<sub>3</sub> were calculated for each spectrum in an image cube from in vivo

reference spectra<sup>21</sup> for oxyhemoglobin, deoxyhemoglobin, and an offset spectrum, respectively, by:

$$\bar{S}_{ij} = \|c_1 \overline{OxyHb} + c_2 \overline{DeoxyHb} + c_3 \overline{Offset}\|_2 \quad (2)$$

These coefficients allowed the determination of total hemoglobin concentration (THb):

$$Total\ Hemoglobin = THb_{ij} = c_{oxyij} + c_{deoxyij} \quad (3)$$

and relative percent saturated oxygen (O<sub>2</sub>sat):

$$\%O_2sat_{ij} = [c_{oxyij}/(THb_{ij})] \times 100 \quad (4)$$

at each pixel location. Grayscale images based on these values were analyzed using standard image analysis techniques. S<sub>HSI</sub>O<sub>2</sub> is calculated as the mean value of %O<sub>2</sub>sat across the region of interest.

## REFERENCES

- Chameides L, Hazinski MF. *Textbook of Pediatric Advanced Life Support*. Dallas, TX: American Heart Association; 1994.
- Carlson KA, Jahr JS. A historical overview and update on pulse oximetry. *Anesthesiol Rev*. 1993;20:173–181.
- Dunham CM, Ransom KJ, Flowers LL, et al. Cerebral hypoxia in severely brain injured patients is associated with admission Glasgow Coma Scale score, computed tomographic severity, cerebral perfusion pressure, and survival. *J Trauma*. 2004;56:482–489.
- Gentilello LM, Sanzone A, Wang L, et al. Near-infrared spectroscopy versus compartment pressure for the diagnosis of lower extremity compartmental syndrome using electromyography-determined measurements of neuromuscular function. *J Trauma*. 2001;51:1–8.
- Beilman GJ, Myers D, Cerra FB, et al. Near-infrared and nuclear magnetic resonance spectroscopic assessment of tissue energetics in an isolated, perfused canine hind limb model of dysoxia. *Shock*. 2001;15:392–397.
- McKinley BA, Marvin RG, Cocanour CS, et al. Tissue hemoglobin O<sub>2</sub> saturation during resuscitation of traumatic shock monitored using near infrared spectrometry. *J Trauma*. 2000;48:637–642.
- Beilman GJ, Groehler KE, Lazaron V, et al. Near-infrared spectroscopy measurement of regional tissue oxyhemoglobin saturation during hemorrhagic shock. *Shock*. 1999;12:196–200.
- Colarusso P, Kidder LH, Levin IW et al. Infrared spectroscopic imaging: from planetary to cellular systems. *Appl Spectrosc*. 1998; 52:106A–120A.
- Paschalis EP, Verdelis K, Doty SB, et al. Spectroscopic characterization of collagen cross-links in bone. *J Bone Miner Res*. 2001;16:1821–1828.
- Potter K, Kidder LH, Levin IW, et al. Imaging of collagen and proteoglycan in cartilage sections using Fourier transform infrared spectral imaging. *Arthritis Rheum*. 2001;44:846–855.
- Zuzak KJ, Schaeberle MD, Gladwin MT et al. Noninvasive determination of spatially resolved and time-resolved tissue perfusion in humans during nitric oxide inhibition and inhalation by use of a visible-reflectance hyperspectral imaging technique. *Circulation*. 2001;104:2905–2910.
- Zuzak KJ, Gladwin MT, Cannon RO 3rd, et al. Imaging hemoglobin oxygen saturation in sickle cell disease patients using noninvasive visible reflectance hyperspectral techniques: effects of nitric oxide. *Am J Physiol Heart Circ Physiol*. 2003;285:H1183–H1189.
- Zuzak KJ, Schaeberle MD, Lewis EN et al. Visible reflectance hyperspectral imaging: characterization of a noninvasive, in vivo

- system for determining tissue perfusion. *Anal Chem.* 2002;74:2021–2028.
14. Greenman RL, Panasyuk S, Wang X et al. Early changes in the skin microcirculation and muscle metabolism of the diabetic foot. *Lancet.* 2005;366:1711–1717.
  15. Payette JR, Sowa MG, Germscheid SL, et al. Noninvasive diagnostics: predicting flap viability with near-IR spectroscopy and imaging. *Am Clin Lab.* 1999;18:4–6.
  16. Stranc MF, Sowa MG, Abdulrauf B, et al. Assessment of tissue viability using near-infrared spectroscopy. *Br J Plast Surg.* 1998;51:210–217.
  17. Sowa MG, Leonardi L, Payette JR, et al. Near infrared spectroscopic assessment of hemodynamic changes in the early post-burn period. *Burns.* 2001;27:241–249.
  18. Leonardi L, Sowa MG, Payette JR, et al. Near-infrared spectroscopy and imaging: a new approach to assess burn injuries. *Am Clin Lab.* 2000;19:20–22.
  19. Gillies R, Freeman JE, Cancio LC, et al. Systemic effects of shock and resuscitation monitored by visible hyperspectral imaging. *Diabetes Technol Therap.* 2003;5:847–855.
  20. Mansfield JR, Sowa MG, Scarth GB, et al. Fuzzy C-means clustering and principal component analysis of time series from near-infrared imaging of forearm ischemia. *Comput Med Imaging Graph.* 1997;21:299–308.
  21. Prall S. Optical absorption of hemoglobin. Oregon Medical Laser Center. Available at: <http://omlc.ogi.edu/spectra/hemoglobin>. Accessed January 12, 2006.
  22. Hettrick DA, Pagel PS, Warltier DC. Desflurane, sevoflurane, and isoflurane impair canine left ventricular-arterial coupling and mechanical efficiency. *Anesthesiology.* 1996;85:403–413.
  23. Muzi M, Ebert TJ. A comparison of baroreflex sensitivity during isoflurane and desflurane anesthesia in humans. *Anesthesiology.* 1995;82:919–925.
  24. Pac-Soo CK, Ma D, Wang C, et al. Specific actions of halothane, isoflurane and desflurane on sympathetic activity and A delta and C somatosympathetic reflexes recorded in renal nerves in dogs. *Anesthesiology.* 1999;91:470–478.
  25. Arain SR, Williams DJ, Robinson BJ, et al. Vascular responsiveness to brachial artery infusions of phenylephrine during isoflurane and desflurane anesthesia. *Anesth Analg.* 2002;94:1137–1140.
  26. Sessler DI, McGuire J, Moayeri A, et al. Isoflurane-induced vasodilation minimally increases cutaneous heat loss. *Anesthesiology.* 1991;74:226–232.
  27. Braverman IM. The cutaneous microcirculation: ultrastructure and microanatomical organization. *Microcirculation.* 1997;4:329–340.
  28. Braverman IM, Schechner JS, Silverman DG, et al. Topographic mapping of the cutaneous microcirculation using two outputs of laser-Doppler flowmetry: flux and the concentration of moving blood cells. *Microvasc Res.* 1992;44:33–48.
  29. Schechner JS, Braverman IM. Synchronous vasomotion in the human cutaneous microvasculature provides evidence for central modulation. *Microvasc Res.* 1992;44:27–32.
  30. Wardell K, Braverman IM, Silverman DG, et al. Spatial heterogeneity in normal skin perfusion recorded with laser Doppler imaging and flowmetry. *Microvasc Res.* 1994;48:26–38.
  31. Stauss HM, Stegmann JU, Persson PB, et al. Frequency response characteristics of sympathetic transmission to skin vascular smooth muscles in rats. *Am J Physiol.* 1999;277:R591–R600.
  32. Gniadecki R, Gniadecka M, Serup J. Examination of periodic fluctuations in cutaneous blood flow. In: Serup J, Jemec GB, eds. *Handbook of Non-Invasive Methods and the Skin*. Boca Raton, FL: CRC Press LLC; 1995:411–420.
  33. Berne C, Fagius J. Skin nerve sympathetic activity during insulin-induced hypoglycaemia. *Diabetologia.* 1986;29:855–860.
  34. Roddie IC. Circulation to skin and adipose tissue. In: Shepherd JT, Abboud FM, eds. *Handbook of Physiology. Section 2: The Cardiovascular System. Volume III. Peripheral Circulation and Organ Blood Flow, Part I*. Bethesda, MD: American Physiological Society; 1983:285–317.
  35. Rowell LB. Cardiovascular adjustments to thermal stress. In: Shepherd JT, Abboud FM, eds. *Handbook of Physiology. Section 2: The Cardiovascular System. Volume III. Peripheral Circulation and Organ Blood Flow, Part I*. Bethesda, MD: American Physiological Society; 1983:967–979.
  36. Bornmyr S, Castenfors J, Evander E, et al. Effect of local cold provocation on systolic blood pressure and skin blood flow in the finger. *Clin Physiol.* 2001;21:570–575.
  37. Bornmyr S, Castenfors J, Svensson H, et al. Detection of autonomic sympathetic dysfunction in diabetic patients. A study using laser Doppler imaging. *Diabetes Care.* 1999;22:593–597.
  38. Sowa MG, Payette JR, Mantsch HH. Near-infrared spectroscopic assessment of tissue hydration following surgery. *J Surg Res.* 1999;86:62–69.
  39. Sowa MG, Matas A, Schattka BJ, et al. Spectroscopic assessment of cutaneous hemodynamics in the presence of high epidermal melanin concentration. *Clin Chim Acta.* 2002;317:203–212.
  40. Light TD, Jeng JC, Jain AK, et al. The 2003 Carl A Moyer Award: real-time metabolic monitors, ischemia-reperfusion, titration endpoints, and ultraprecise burn resuscitation. *J Burn Care Rehabil.* 2004;25:33–44.